

Constraining Galactic Structure with the LISA White Dwarf Foreground

KATELYN BREIVIK,¹ CHIARA M. F. MINGARELLI,^{2,3} AND SHANE L. LARSON^{4,5}

¹*Canadian Institute for Theoretical Astrophysics, University of Toronto, 60 St. George Street, Toronto, Ontario, M5S 1A7, Canada*

²*Center for Computational Astrophysics, Flatiron Institute, 162 Fifth Ave, New York, NY, 10010, USA*

³*Department of Physics, University of Connecticut, 196 Auditorium Road, U-3046, Storrs, CT 06269-3046, USA*

⁴*Center for Interdisciplinary Exploration & Research in Astrophysics (CIERA), Northwestern University, 1800 Sherman Ave, Evanston, Illinois 60201, USA*

⁵*Department of Physics & Astronomy, Northwestern University, 2145 Sheridan Road, Evanston, Illinois 60208-3112, USA*

(Revised December 6, 2019)

ABSTRACT

White dwarfs comprise 95% of all stellar remnants, and are thus an excellent tracer of old stellar populations in the Milky Way. Current and planned telescopes are not able to directly probe the white dwarf population in its entirety due to its inherently low luminosity. However, the Galactic population of double white dwarf binaries gives rise to a millihertz gravitational-wave foreground detectable by the Laser Interferometer Space Antenna (LISA). Here we show how characterizing this foreground’s angular power spectrum will enable us to probe the Galactic structure in a novel way and measure the vertical scale height of the Galaxy’s oldest stellar populations. We do this using a binary population synthesis study that incorporates different Galactic spatial distributions for the double white dwarf population. We find that the level of anisotropy in the white dwarf foreground’s angular power spectrum is strongly dependent on the vertical scale height of the population. Finally, we show that LISA can probe the vertical scale height of the Galactic double white dwarf population with an accuracy of 50 pc – 200 pc, depending on angular resolution limits, using the angular power spectrum of the white dwarf foreground.

Keywords: white dwarfs – gravitational waves – Milky Way disk

1. INTRODUCTION

The scale heights of Galactic stellar populations are a direct probe of dynamical interactions over the age of the Milky Way. Different scale heights as a function of radius can test dark matter models (e.g. Church et al. 2019), the Milky Way’s minor merger history (e.g. Villalobos & Helmi 2008), the strength of tidal interactions from close interactions (e.g. Bensby & Feltzing 2010), or constant heating through effects from the dynamical quadrupole of the Galactic bar (e.g. Grand et al. 2016). Since dynamical interactions are expected to occur on Gyr timescales, old stellar populations are excellent candidates for scale height measurements which trace the dynamical evolution of the Galaxy (e.g. Belokurov 2013). However, these populations are dim and

thus difficult to observe electromagnetically throughout the Galaxy. So far, the most precise Galactic structure measurements come from fitting data from electromagnetic surveys to Galactic population synthesis simulations, (e.g. Robin et al. 2003; Jurić et al. 2008; McMillan 2011; Gao et al. 2013; Pieres et al. 2019). These surveys have limited fields of view and observe mostly young, bright sources due to magnitude limits. Thus they do not fully probe the structure of the dimmest, oldest populations.

Double white dwarf (DWD) systems are an interesting probe of the scale heights of Galactic populations since they are the remnants of low-mass stellar progenitors which make up 95% of total population. Furthermore, the population of DWDs is necessarily old since it is born from stellar progenitors with Gyr lifetimes. Importantly, gravitational wave (GW) signals from long-lived inspiraling DWDs are not suppressed or obscured by gas, dust, or other stars in the Galaxy, as their elec-

tromagnetic counterparts may be. GWs are therefore an excellent way of observing the Galactic population of DWDs and its spatial structure.

The incoherent superposition of GW signals from the Galactic DWDs form a loud foreground in the millihertz GW frequency band, detectable by the Laser Interferometer Space Antenna (LISA; e.g. Baker et al. 2019a). The LISA WD foreground signal has long been considered a nuisance, with significant effort being devoted to subtracting it (e.g. Robson & Cornish 2017). Here we treat this foreground as a loud signal which can be used to constrain the scale height of the Galactic disk. Benacquista & Holley-Bockelmann (2006) and Korol et al. (2019) have previously investigated LISA’s ability to constrain Galactic structure from GW observations of the WD foreground. Specifically, Benacquista & Holley-Bockelmann (2006) studied the 1-D shape of the power spectral density (PSD) of the WD foreground to try to measure the vertical scale height of the Galactic disk. Their constraints depend heavily on the estimated number density of DWDs in the Galaxy – which is only well understood locally (Toonen et al. 2017). Korol et al. (2019) predict that individual, well-localized DWDs across the Galaxy can precisely trace the Galactic scale height. However, these well-measured DWDs originate from a small subset of the total DWD population because resolved GW measurements are biased toward more massive, shorter period, or nearby binaries (Lamberts et al. 2019).

Here, we show that the *angular* power spectrum of the WD foreground contains an imprint of the spatial structure of the DWD population. The WD foreground is an excellent, and less biased, probe of this structure since the entire Galactic DWD population contributes to it. Specifically, we take a similar approach to Pulsar Timing Array (PTA) (Mingarelli et al. 2013; Taylor et al. 2015), and LIGO/Virgo GW background anisotropy studies (Thrane et al. 2009), and decompose the foreground on a basis of spherical harmonics. We find that the angular power spectra of WD populations with different spatial distributions vary significantly. We show that it is possible to constrain the scale height of the DWD population to an accuracy of ~ 200 pc using the amplitude and shape of the measured angular power spectrum of the LISA WD foreground. If higher angular resolution is achieved, a vertical scale height measurement accuracy of ~ 50 pc is possible.

The organization of the paper is as follows: in Section 2 we review the calculation of GW signals from DWDs, in Section 3 we describe our simulations of the Galactic population of DWDs, in Section 4 we describe how we model the WD foreground anisotropy, in Sec-

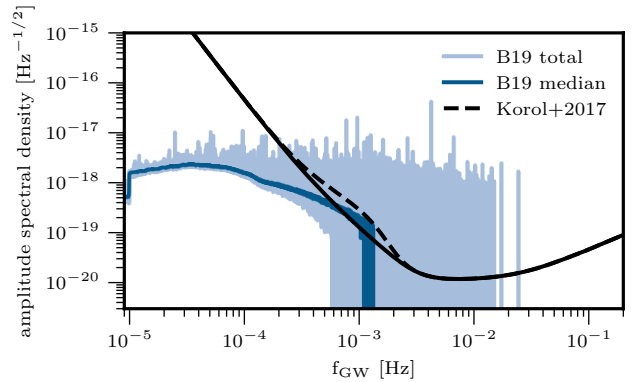


Figure 1. Amplitude spectral density vs gravitational wave frequency, f_{GW} , for the entire DWD population of B19 (light blue), the running median of the population with a window of 100 frequency bins (dark blue), and the fit to the Korol et al. (2017) foreground taken from Robson et al. (2019) (dashed). The running median of B19 population is comparable to the Korol et al. (2017) foreground.

tion 5 we report our main results, and we finish with a discussion in Section 6.

2. GWS FROM DWDs

Since we focus on the DWD population only, we assume all sources are circular and do not evolve due to gravitational radiation over a LISA observation time of 4 years. We compute the polarization-averaged dimensionless strain, following Nelemans et al. (2001) as

$$h = 10^{-21} \left(\frac{\mathcal{M}_c}{M_\odot} \right)^{5/3} \left(\frac{P_{\text{orb}}}{\text{hr}} \right)^{-2/3} \left(\frac{D}{\text{kpc}} \right)^{-1}, \quad (1)$$

where $\mathcal{M}_c = (m_1 m_2)^{5/3} / (m_1 + m_2)$ is the chirp mass. For stationary sources the amplitude spectral density (ASD) of a single DWD is

$$ASD = h \sqrt{T_{\text{obs}}}, \quad (2)$$

where we assume $T_{\text{obs}} = 4$ yr.

To find the total GW signal from all DWDs in the Galaxy, we sum the PSD of each DWD, where

$$PSD = ASD^2 = h^2 T_{\text{obs}}. \quad (3)$$

The PSD of the population is binned according to LISA’s frequency resolution of $\Delta f = 1/T_{\text{obs}} \simeq 8 \times 10^{-9}$ Hz such that the PSD for each frequency bin is the sum of the PSD from each DWD occupying that bin. The ASD of the bin is then the square root of the PSD .

The process of subtracting resolved sources from the foreground to produce an irreducible foreground is beyond the scope of this work and is discussed in Robson

& Cornish (2017). Instead, we focus on the GW signal coming from the entire WD foreground. In order to provide a comparison to previous work which has simulated a resolved source subtraction routine (e.g. Korol et al. 2017), we approximate the irreducible foreground by taking a running median of the *PSD* with a window of 100 frequency bins.

Figure 1 shows a comparison of the *ASD* of the LISA noise floor compared to the *ASD* of the DWD population of Breivik et al. (2019), hereafter B19. Since the orbital evolution of the DWD population is driven by GW emission, the orbital evolution scales as $\dot{f}_{\text{orb}} \propto f_{\text{GW}}^{11/3}$. This leads to a pileup of DWDs at lower frequencies. The foreground sharply decreases near 10 mHz because the B19 population removes all mass transferring DWDs. Generally, mass transferring DWDs are expected to occupy higher GW frequencies, and will thus not contribute to the foreground near 1 mHz; see Kremer et al. (2017); Breivik et al. (2018) for a discussion of mass transferring DWDs observable by LISA. Figure 1 also shows the irreducible foreground of Korol et al. (2017) and the running median of the B19 *ASD*. We find general agreement between the two curves, though the B19 running median artificially cuts off the *ASD* near 2 mHz. This cutoff is a direct consequence of the truncation of the B19 foreground at higher frequencies.

3. SIMULATING WHITE DWARF BINARIES IN THE MILKY WAY

We simulate two Milky Way populations of DWDs using COSMIC¹. COSMIC is a community-developed, python-based binary population synthesis suite based on BSE (Hurley et al. 2002) which includes several upgrades to binary interactions and massive star evolution, as well as models for initial binary populations and Galactic spatial distributions (B19). In both populations, we use the binary evolution model described in B19 (see Section 4). In our fiducial model, Model 1, we convolve the simulated binary populations with star formation histories and spatial distributions to generate a thin disk, thick disk, and bulge population, following the procedure detailed in B19. The thin disk is assumed to be formed from constant, solar metallicity star formation over the past 10 Gyr, while the thick disk is assumed have formed from a 1 Gyr burst of uniform, 15%-solar metallicity star formation 11 Gyr in the past. The bulge is assume to have formed 10 Gyr in the past with a 1 Gyr burst of uniform, solar metallicity star formation.

Following B19, the spatial distributions are consistent with McMillan (2011). The thin and thick disks are

assumed to be azimuthally symmetric and distributed radially and vertically as

$$\rho(r)\rho(z) \propto \exp(-r/r_h) \exp(-z/z_h). \quad (4)$$

We assume a radial scale height of $r_h = 2.9$ kpc and a vertical scale height of $z_h = 0.3$ kpc for the thin disk. The thick disk radial and vertical scale heights are $r_h = 3.31$ kpc and $z_h = 0.9$ kpc. The bulge is also assumed to be azimuthally symmetric and distributed radially and vertically as

$$\rho(r') \propto \frac{\exp[-(r/r_{\text{cut}})^2]}{(1+r'/r_0)^\alpha}, \quad (5)$$

where,

$$r' = \sqrt{r^2 + (z/q)^2}, \quad (6)$$

and $\alpha = 1.8$, $r_0 = 0.075$ kpc, $r_{\text{cut}} = 2.1$ kpc, and $q = 0.5$. The mass of the thin disk is assumed to be $M_{\text{thin}} = 4.32 \times 10^{10} M_\odot$; the mass of the thick is assumed to be $M_{\text{thick}} = 1.44 \times 10^{10}$; the mass of the bulge is assumed to be $M_{\text{bulge}} = 8.9 \times 10^9 M_\odot$ (McMillan 2011).

We define a comparison model, Model 2, which uses the same binary evolution, star formation history, and spatial distribution for the thick disk and bulge as Model 1. However, the thin disk population is assigned vertical positions according to Model 1's thick disk scale height of $z_h = 900$ pc. This comparison is designed to test if the GW foreground can be used to confirm whether the DWDs trace the same Galactic distribution as the relatively younger stars observable across the Galaxy by electromagnetic surveys, or if they trace a more dynamically heated distribution associated with old stellar populations in the thick disk. Spatial distributions with larger vertical disk scale heights, without changes to the DWD spatial density or population number, will increase the average distance to the DWD population. This will, in turn, decrease the overall strength of the GW foreground since the GW signal scales inversely with distance (see Equation 1).

Different star formation histories will change the birth time of the DWD population, and thus impact the number of DWDs which radiate in the LISA frequency band (e.g. Lamberts et al. 2019). If the DWD population results from a majority of very early star formation, this will lead to longer GW evolution times and thus a higher rate of WD mergers which will reduce the foreground height and shift it towards higher GW frequencies. Conversely, if the DWD population is formed from primarily late star formation, the GW evolution times will be shorter and result in a foreground only at lower frequencies. Different binary evolution models, particularly those pertaining to common envelope evolution,

¹ cosmic-popsynth.github.io

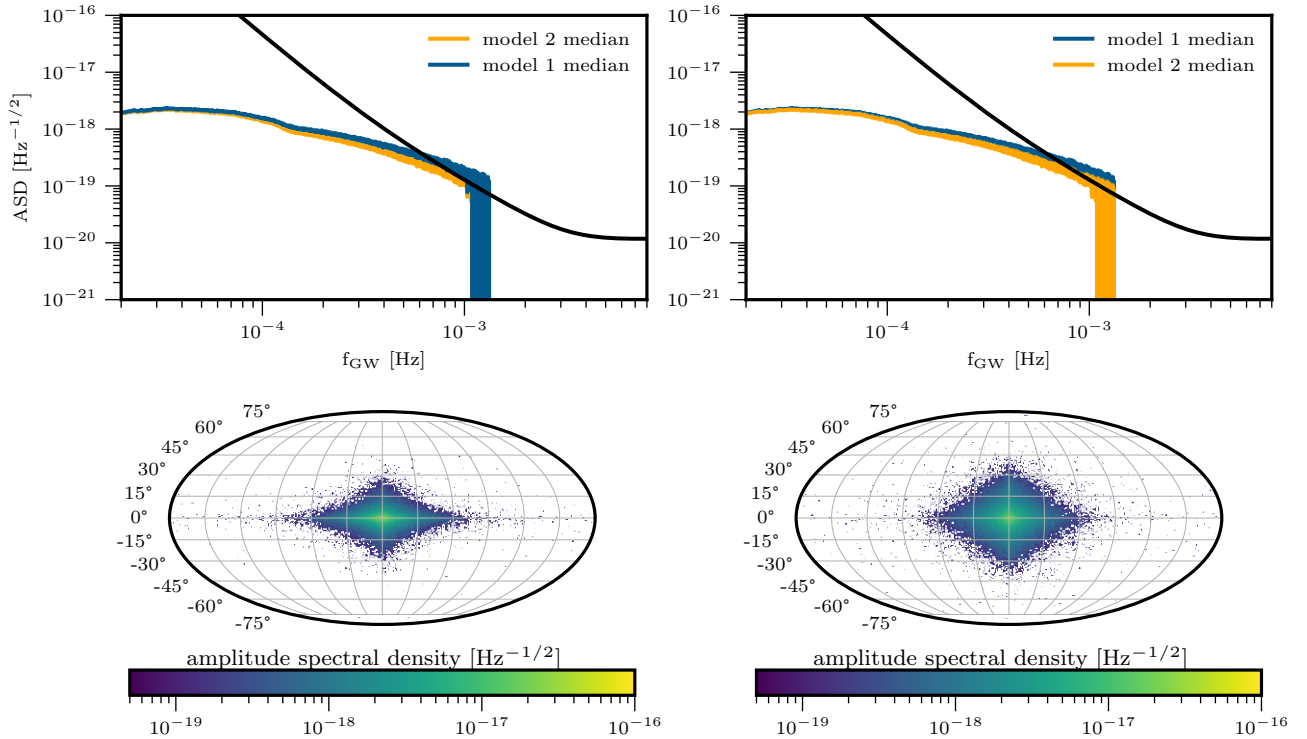


Figure 2. The LISA 1D-amplitude spectral density (ASD; above) and its WD population (below) for Model 1 (left, $z_h = 300$ pc) and Model 2 (right, $z_h = 900$ pc). On the top row, both models are overplotted in each Figure to illustrate the nearly identical ASD. The bottom row shows the ASD in Galactocentric coordinates for all frequencies between 0.1 mHz and 10 mHz. While the 2-D projection of the two models vary significantly (bottom left and right), the ASDs (top left and right) are virtually identical – motivating our new approach.

will also have a strong impact on the GW frequency distribution of the DWD population (e.g. [Kremer et al. 2017](#)). We leave a thorough study of the impact of binary evolution on the angular GW power spectrum of the WD foreground as a topic of future study.

Figure 2 shows the comparison between the 1-D *ASD* running median of the WD foreground (top row) and the 2-D projection of the WD foreground’s *ASD* in Galactocentric coordinates (bottom row) from Model 1 and Model 2. The differences between each model are barely distinguishable when comparing the 1-D *ASDs*, thus motivating the need for alternative approaches to measuring the vertical scale height of the DWD population with the WD foreground. The differences between each model when considering the 2-D projection of the *ASD* onto the sky, however, are very obvious. Distributing all disk DWDs in a thick disk results in GW signals distributed much more widely across the sky. This suggests a strong potential for inferring the WD foreground’s spatial structure by its *angular* GW power spectrum.

4. WD FOREGROUND ANISOTROPY

While [Benacquista & Holley-Bockelmann \(2006\)](#) studied the differences in the WD foreground *PSD* as a func-

tion of vertical disk scale height, here we decompose the WD foreground on a basis of spherical harmonics to examine its angular power spectrum. This is a well-known approach to characterizing both electromagnetic and GW backgrounds. For example, anisotropy in the nanohertz GW background (accessible with PTAs) is likely generated by nearby unresolved supermassive BH binaries (SMBHBs), and/or excess GW power coming from galaxy clusters where there may be many merging SMBHBs ([Mingarelli et al. 2017](#)). Various astrophysical GW signals could add incoherently and generate an anisotropic GW background signal in the LIGO/Virgo band (e.g. [Thrane et al. 2009](#); [Romano et al. 2015](#); [Jenkins et al. 2019](#); [Renzini & Contaldi 2019a,b](#)). Similar to LIGO/Virgo, several astrophysical or cosmological GW signals could produce an anisotropic GW background in the LISA band ([Giampieri & Polnarev 1997](#); [Ungarelli & Vecchio 2001](#); [Cornish 2001](#); [Kudoh & Taruya 2005](#); [Taruya & Kudoh 2005](#); [Romano & Cornish 2017](#)), including the Galactic DWD population ([Seto & Cooray 2004](#); [Conneely et al. 2019](#)).

We use the populations discussed in Section 3 and their *PSDs* to compute the angular power spectrum for each model. Each DWD’s *PSD* is captured in a pixel

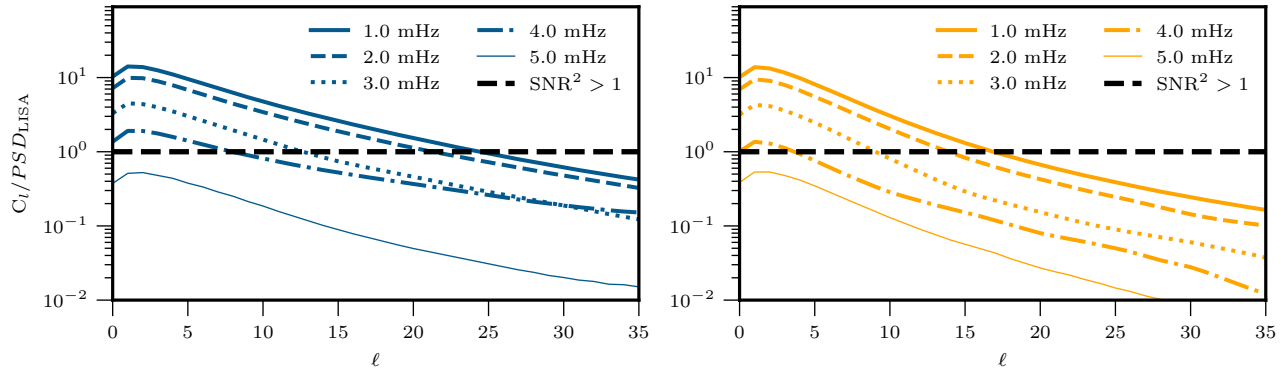


Figure 3. The ratio of the angular power spectrum to the LISA sensitivity for 5 frequency slices denoted by different line styles for Model1 (left) and Model2 (right). Each slice has a width of 1mHz and is binned by the left edge such that $f_{\text{GW}} = 1$ mHz represents the slice from 1 mHz to 2mHz. The angular power spectrum is observable if $C_\ell/PSD_{\text{LISA}} > 1$ (grey dashed line), thus the angular power spectrum of each model is observable up to $\ell = 10$ for $f_{\text{GW}} \leq 3$ mHz.

of a HEALPix sky map (we use $\text{NSIDE} = 128$, corresponding to 196,609 pixels) for a given GW frequency. The total power on the sky is 4π , and is decomposed as

$$P(\hat{\Omega}) = \sum_{\ell, m} c_{\ell m} Y_{\ell m}, \quad (7)$$

where $\hat{\Omega}$ is the direction of GW propagation, and the $Y_{\ell m}$ are the spherical harmonics. We describe the anisotropy of the foreground in terms of the angular power spectrum

$$C_\ell = \sum_{m=-\ell}^{+\ell} \frac{|c_{\ell m}|^2}{2\ell + 1}, \quad (8)$$

and normalize to the isotropic component, C_0 , as in Taylor et al. (2015); Mingarelli et al. (2017).

In this study, we compute the angular power spectrum of the LISA WD foreground with realistic Galactic DWD population models. While not explored here, the annual modulation of the GW power in the WD foreground due to LISA’s motion in its Earth-trailing orbit (Seto 2004) will aid in the Galactic scale height measurement since extra pointing information will be encoded in the foreground modulation. Furthermore, we do not consider the full LISA analysis framework for measuring the angular power spectrum of the DWD’s GW foreground. For a detailed description of the application of this technique to LISA data we refer the reader to Cornish (2001); Seto & Cooray (2004); Kudoh & Taruya (2005); Taruya & Kudoh (2005); Baker et al. (2019b).

We show the angular power spectrum from 5 GW frequency slices with a 1mHz width created from the populations of Model1 and Model2 in Figure3. The frequency slice width of 1mHz allows for a stronger GW signal, and thus better resolution of the foreground anisotropy. For each frequency slice, we evaluate the

LISA PSD to show which multipole moments from our WD Foreground models are detectable above the LISA noise floor (i.e. where $C_\ell/PSD_{\text{LISA}} > 1$). The angular power spectra of the 1 – 3 mHz frequency slices will be well resolved up to $\ell \sim 10$, with the strongest signal coming from the lowest frequencies.

5. RESULTS

We propose to use the difference between the angular GW power spectra from different scale height models to probe the scale height of the Galaxy. We begin by considering the difference of the spectra between Model1 and Model2: $(C_\ell/C_0)_1 - (C_\ell/C_0)_2$. We compute the angular power spectra for both models and the difference between them at 40 frequency slices between 1 mHz to 3 mHz. Each slice is spaced at 0.05 mHz intervals and has a width of 1 mHz. Figure4 shows the angular GW power spectra from each model (top), and the difference between the angular power spectra from each model (bottom). The solid lines show the mean of the 40 frequency slices and the shaded regions show the 1σ spread around the mean. The dashed lines in Figure4 show a representative angular resolution of $\ell = 4$ for LISA at $f_{\text{GW}} \sim 1$ mHz (e.g. Ungarelli & Vecchio 2001; Cornish 2001; Seto & Cooray 2004; Baker et al. 2019b). We do not consider the foreground at $f_{\text{GW}} > 3$ mHz because the angular power spectrum is not expected to be strongly resolved by LISA in either model.

The level of anisotropy scales directly with the scale height of the DWD population: models with smaller disk scale heights distribute WDs more anisotropically and thus produce more anisotropic GW foregrounds than models with lower disk scale heights. Indeed, Model1, which distributes the DWDs more closely to the plane of the Galaxy, results in a more anisotropic GW foreground with more power at higher multipoles relative

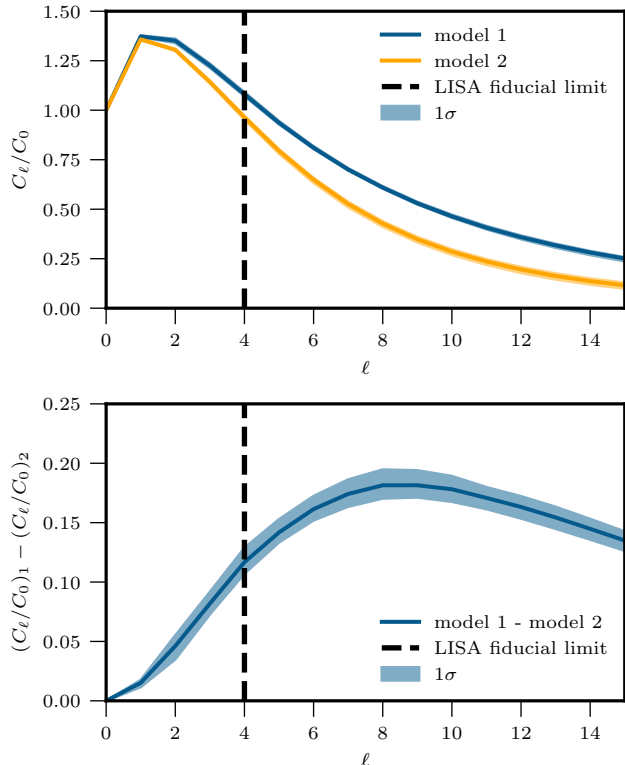


Figure 4. The top panel shows the mean anisotropic angular power spectrum, and 1σ spread from 40 frequency slices with a 1 mHz width ranging from 1 mHz to 3 mHz for Model 1 and Model 2. The bottom panel shows the difference of the angular power spectra from each model, and the 1σ spread from the 40 frequency slices. The dotted line in each plot shows a representative angular resolution for LISA at mHz frequencies. The difference between Model 1 and Model 2 is resolved for $\ell \leq 4$ and thus distinguishable with LISA’s angular resolution.

to Model 2. Importantly, the anisotropy of both populations is maintained in each frequency slice indicating that this is a robust method for scale height measurement.

Once LISA is operational, models for the angular power spectrum using different scale heights can be fit to the observed angular power spectrum to infer the DWD population’s scale height. A Galactic scale height measurement is possible with LISA’s current configuration at low multipoles ($\ell \sim 4$). However, the largest differences between Model 1 and Model 2 occur at $\ell \simeq 8$, which is well above the resolution of a single LISA detector. The most straightforward way to achieve this resolution is through two space-based GW observatories operating simultaneously (e.g. Baker et al. 2019b).

The DWDs from Model 2 in the thin disk are distributed with a vertical scale height of $z_h = 900$ pc

as a proof of concept. To investigate the resolution with which LISA can determine the vertical scale height of the Galactic DWD population, we repeat the process detailed above for vertical scale heights between $z_h = 300$ pc and $z_h = 900$ pc at 50 pc intervals. We compare the difference between the power spectra of Model 1 and each population: $(C_\ell/C_0)_1 - (C_\ell/C_0)_{z_h}$.

The left panel of Figure 5 shows the mean difference between the angular power spectra for Model 1 and models with vertical scale heights $z_h = 400$ pc, $z_h = 600$ pc, and $z_h = 800$ pc. As the scale height increases from 400 pc to 800 pc, the difference between the power spectra deviate farther from 0. This deviation serves as a proxy for LISA’s resolution to the scale height of the DWD population. While the difference between Model 1 and the population with $z_h = 400$ pc is very near zero, the populations with scale heights $z_h = 600$ pc and $z_h = 800$ pc have mean differences well above zero at $\ell \leq 4$ thus indicating that a scale height measurement is possible.

The right panel of Figure 5 shows the multipole where the 3σ spread of the difference between the angular power spectra of Model 1 and models with different scale heights deviates from 0 and is thus distinguished by LISA. LISA is unable to distinguish between models where the 3σ spread of the difference is consistent with 0. As the population scale height increases, the multipole required to resolve the population as distinct from Model 1 decreases. All populations with scale heights $z_h > 500$ pc are distinguishable with LISA’s angular resolution of $\ell = 4$ which implies a scale height measurement accuracy of ~ 200 pc. At an angular resolution of $\ell = 40$, the scale height measurement is possible with an accuracy of 50 pc. In comparison, Korol et al. (2019) find that LISA can measure the scale height of the disk to an accuracy of 80 pc using observations of resolved DWDs. These GW-based techniques provide comparable resolution to electromagnetic measurements which measure the thin and thick disk scale heights to a precision of 10 pc – 50 pc (e.g. Robin et al. 2003; McMillan 2011; Gao et al. 2013; Pieres et al. 2019). However, due to the inherently dim nature of WDs, electromagnetic surveys are unable to measure the WD population’s structure across the Galaxy.

6. DISCUSSION

The WD foreground is a rich astrophysical GW source in the mHz frequency regime. Here, we have shown that the angular GW power spectrum of the WD foreground can be used to infer the vertical scale height of the Galactic DWD population. Since WDs are dim, a scale height measurement of the WD population is difficult to make

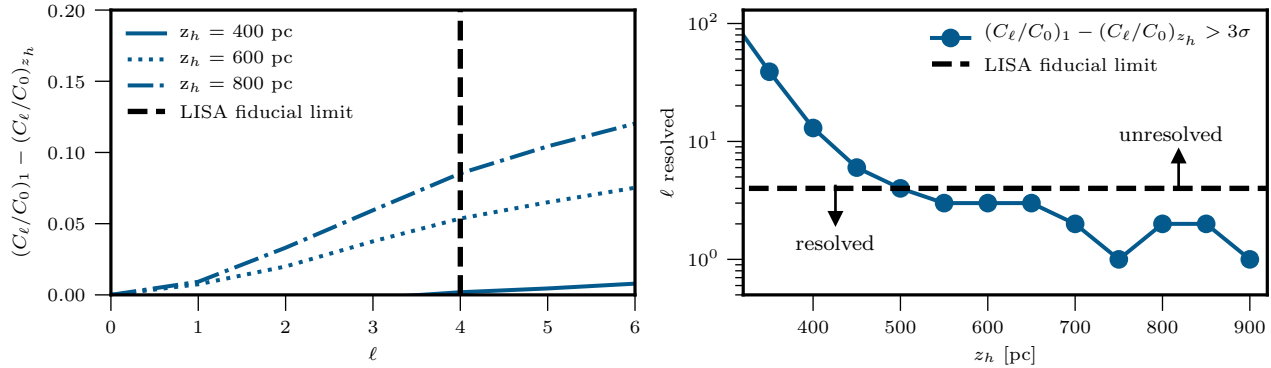


Figure 5. The difference between the angular power spectra of populations with thin disk scale heights $z_h = 400$ pc, 600 pc, and 800 pc and the angular GW power spectrum of Model 1 ($z_h = 300$ pc, left) and the multipole where the 3σ spread of the difference of the angular power spectra deviates from 0 as a function of scale height (right). The black dotted line shown in each plot shows a representative angular resolution for LISA at mHz frequencies. The difference between the angular power spectra relative to Model 1 increases with the disk scale height (left) and is resolved at $\ell \leq 4$ for $z_h \geq 500$ pc (right) which corresponds to a disk scale height measurement resolution of 200 pc. A scale height measurement resolution of 50 pc is attainable at the angular resolution of $\ell = 40$.

with electromagnetic surveys. By considering the angular power spectrum of the WD foreground, our technique avoids both obscuration by dust, gas, and other stars as well as observational biases toward short period, high mass, and/or nearby resolved DWDs.

We used two models to illustrate how the angular power spectrum can be used to measure the vertical disk scale height of the Galactic DWD population. Model 1 is taken directly from the DWD population of B19 which assumes a thin disk, thick disk, and bulge population. Model 2 assumes the same star formation history, binary evolution models, and spatial distributions for the thick disk and bulge as Model 1, but vertically distributes all thin disk DWDs according to the spatial distribution of Model 1’s thick disk. We showed that the 1-D *PSD* of these two populations is nearly identical, but that the 2-D distribution of the *PSD* is highly anisotropic, and significantly different between the models (Figure 2). We then decomposed the GW foreground of each model on a basis of spherical harmonics to create their angular power spectra. We find that the angular power spectral shape is very likely observable by LISA and robust across GW frequencies from 1 mHz to 3 mHz (Figure 3). We show that the difference between these angular power spectra can be used to quantify differences between DWD populations with different scale heights (Figure 4). This presents a complementary approach to scale height measurements made through electromagnetic observations, the 1-D GW *PSD*, or DWDs resolved by LISA with similar resolution.

We applied this new technique to several populations with scale heights varying from $z_h = 300$ pc to $z_h = 900$ pc to determine LISA’s ability to resolve the

vertical disk scale height of the population of Galactic DWDs (Figure 5). We find that LISA, at its current resolution limits, is capable of resolving between DWD scale height models to an accuracy of ~ 200 pc which is comparable to the resolution of the other measurement techniques within a factor of 3 – 10. A vertical scale height measurement accuracy of ~ 200 pc is attainable at angular resolutions of $\ell \geq 40$, thus motivating the demand for higher angular resolution which can be achieved through two simultaneously operating space-based GW observatories.

Any scale height measurements of the DWD population, which traces some of the oldest stellar populations in the Galaxy, are only possible through GW observations. The Galactic WDs are either too dim for electromagnetic surveys or obscured by gas and dust. While GW observations of resolved DWDs can measure the vertical scale height of the WD population to an accuracy of 80 pc, these resolved sources could be biased towards high frequency, more massive, or nearby systems. The angular GW power spectrum of the WD foreground offers a new, less biased, way to measure the vertical scale height of the Galactic DWD population.

7. ACKNOWLEDGEMENTS

The authors are grateful for helpful discussions with Renée Hložek and Alberto Sesana. K.B. acknowledges support from the Jeffery L. Bishop Fellowship. Some of the results in this paper have been derived using the healpy and HEALPix package. The Flatiron Institute is supported by the Simons Foundation.

Software: Astropy (Astropy Collaboration et al. 2013, 2018), Healpy (Zonca et al. 2019), COSMIC (Breivik et al. 2019; Breivik et al. 2019), Matplotlib (Hunter 2007),

Numpy (van der Walt et al. 2011), NX01 (Taylor & Baker 2017), Pandas (McKinney 2010), SciPy (Virtanen et al. 2019)

REFERENCES

- Astropy Collaboration, Robitaille, T. P., Tollerud, E. J., et al. 2013, *A&A*, 558, A33
- Astropy Collaboration, Price-Whelan, A. M., Sipőcz, B. M., et al. 2018, *AJ*, 156, 123
- Baker, J., Bellovary, J., Bender, P. L., et al. 2019a, arXiv e-prints, arXiv:1907.06482
- Baker, J., Baker, T., Carbone, C., et al. 2019b, arXiv e-prints, arXiv:1908.11410
- Belokurov, V. 2013, *NewAR*, 57, 100
- Benacquista, M., & Holley-Bockelmann, K. 2006, *ApJ*, 645, 589
- Bensby, T., & Feltzing, S. 2010, in *IAU Symposium*, Vol. 265, *Chemical Abundances in the Universe: Connecting First Stars to Planets*, ed. K. Cunha, M. Spite, & B. Barbuy, 300–303
- Breivik, K., Kremer, K., Bueno, M., et al. 2018, *ApJL*, 854, L1
- Breivik, K., Coughlin, S. C., Zevin, M., et al. 2019, arXiv e-prints, arXiv:1911.00903
- Breivik, K., Coughlin, S. C., Zevin, M., et al. 2019, *COSMIC-PopSynth/COSMIC: COSMIC*, vv3.2.0, Zenodo, doi:10.5281/zenodo.3561144. <https://doi.org/10.5281/zenodo.3561144>
- Church, B. V., Mocz, P., & Ostriker, J. P. 2019, *MNRAS*, 485, 2861
- Conneely, C., Jaffe, A. H., & Mingarelli, C. M. F. 2019, *MNRAS*, 487, 562
- Cornish, N. J. 2001, *Classical and Quantum Gravity*, 18, 4277
- Gao, S., Just, A., & Grebel, E. K. 2013, *A&A*, 549, A20
- Giampieri, G., & Polnarev, A. G. 1997, *MNRAS*, 291, 149
- Grand, R. J. J., Springel, V., Gómez, F. A., et al. 2016, *MNRAS*, 459, 199
- Hunter, J. D. 2007, *Computing in Science Engineering*, 9, 90
- Hurley, J. R., Tout, C. A., & Pols, O. R. 2002, *MNRAS*, 329, 897
- Jenkins, A. C., Romano, J. D., & Sakellariadou, M. 2019, *PhRvD*, 100, 083501
- Jurić, M., Ivezić, Ž., Brooks, A., et al. 2008, *ApJ*, 673, 864
- Korol, V., Rossi, E. M., & Barausse, E. 2019, *MNRAS*, 483, 5518
- Korol, V., Rossi, E. M., Groot, P. J., et al. 2017, *MNRAS*, 470, 1894
- Kremer, K., Breivik, K., Larson, S. L., & Kalogera, V. 2017, *ApJ*, 846, 95
- Kudoh, H., & Taruya, A. 2005, *PhRvD*, 71, 024025
- Lamberts, A., Blunt, S., Littenberg, T. B., et al. 2019, *MNRAS*, 2426
- McKinney, W. 2010, in *Proceedings of the 9th Python in Science Conference*, ed. S. van der Walt & J. Millman, 51 – 56
- McMillan, P. J. 2011, *MNRAS*, 414, 2446
- Mingarelli, C. M. F., Sidery, T., Mandel, I., & Vecchio, A. 2013, *PhRvD*, 88, 062005
- Mingarelli, C. M. F., Lazio, T. J. W., Sesana, A., et al. 2017, *Nature Astronomy*, 1, 886
- Nelemans, G., Yungelson, L. R., & Zwart, S. F. P. 2001, *A&A*, 375, 890
- Pieres, A., Girardi, L., Balbinot, E., et al. 2019, arXiv e-prints, arXiv:1904.04350
- Renzini, A. I., & Contaldi, C. R. 2019a, *PhRvL*, 122, 081102
- . 2019b, *PhRvD*, 100, 063527
- Robin, A. C., Reylé, C., Derrière, S., & Picaud, S. 2003, *A&A*, 409, 523
- Robson, T., & Cornish, N. 2017, *Classical and Quantum Gravity*, 34, 244002
- Robson, T., Cornish, N. J., & Liu, C. 2019, *Classical and Quantum Gravity*, 36, 105011
- Romano, J. D., & Cornish, N. J. 2017, *Living Reviews in Relativity*, 20, 2
- Romano, J. D., Taylor, S. R., Cornish, N. J., et al. 2015, *PhRvD*, 92, 042003
- Seto, N. 2004, *PhRvD*, 69, 123005
- Seto, N., & Cooray, A. 2004, *PhRvD*, 70, 123005
- Taruya, A., & Kudoh, H. 2005, *PhRvD*, 72, 104015
- Taylor, S., & Baker, P. T. 2017, doi:10.5281/zenodo.250258
- Taylor, S. R., Mingarelli, C. M. F., Gair, J. R., et al. 2015, *PhRvL*, 115, 041101
- Thrane, E., Ballmer, S., Romano, J. D., et al. 2009, *PhRvD*, 80, 122002
- Toonen, S., Hollands, M., Gänsicke, B. T., & Boekholt, T. 2017, *A&A*, 602, A16
- Ungarelli, C., & Vecchio, A. 2001, *PhRvD*, 64, 121501
- van der Walt, S., Colbert, S. C., & Varoquaux, G. 2011, *Computing in Science Engineering*, 13, 22

Villalobos, ., & Helmi, A. 2008, Monthly Notices of the
Royal Astronomical Society, 391, 1806.

<https://doi.org/10.1111/j.1365-2966.2008.13979.x>

Virtanen, P., Gommers, R., Oliphant, T. E., et al. 2019,
arXiv e-prints, arXiv:1907.10121

Zonca, A., Singer, L., Lenz, D., et al. 2019, Journal of Open
Source Software, 4, 1298.

<http://dx.doi.org/10.21105/joss.01298>